



**HAL**  
open science

# Edge mode spectroscopy of fractional Chern insulators

F. Binanti, N. Goldman, C. Repellin

► **To cite this version:**

F. Binanti, N. Goldman, C. Repellin. Edge mode spectroscopy of fractional Chern insulators. 2023.  
hal-04268553

**HAL Id: hal-04268553**

**<https://hal.science/hal-04268553v1>**

Preprint submitted on 2 Nov 2023

**HAL** is a multi-disciplinary open access archive for the deposit and dissemination of scientific research documents, whether they are published or not. The documents may come from teaching and research institutions in France or abroad, or from public or private research centers.

L'archive ouverte pluridisciplinaire **HAL**, est destinée au dépôt et à la diffusion de documents scientifiques de niveau recherche, publiés ou non, émanant des établissements d'enseignement et de recherche français ou étrangers, des laboratoires publics ou privés.

# Edge mode spectroscopy of fractional Chern insulators

F. Binanti,<sup>1</sup> N. Goldman,<sup>2</sup> and C. Repellin<sup>1</sup>

<sup>1</sup>*Univ. Grenoble-Alpes, CNRS, LPMMC, 38000 Grenoble, France*

<sup>2</sup>*CENOLI, Université Libre de Bruxelles, CP 231, Campus Plaine, B-1050 Brussels, Belgium*

(Dated: June 5, 2023)

The exploration of atomic fractional quantum Hall (FQH) states is now within reach in optical-lattice experiments. While bulk signatures have been observed in a system realizing the Hofstadter-Bose-Hubbard model in a box [Leonard et al., arXiv:2210.10919], how to access hallmark edge properties in this setting remains a central open question. We propose and analyze a realistic scheme to extract the momentum-resolved edge spectrum of atomic FQH states. Our proposal is based on subjecting the prepared FQH ground state to two interfering Laguerre-Gaussian beams, which transfer a controlled angular momentum  $l$  and energy  $\hbar\omega$  to the system. The resonant coupling is then detected through local density measurements, by tracking the transfer of atoms from the bulk to the edge of the FQH droplet. We benchmark our method using numerical simulations of the Hofstadter-Bose-Hubbard model, considering few bosons in the  $\nu = 1/2$  Laughlin ground state. These studies demonstrate that our probing scheme is well suited to extract hallmark features of FQH spectra: a chiral gapless edge branch and a gapped magneto-roton mode. These signatures are already detectable in realistic systems of two bosons, provided that the box potential is larger than the droplet. Our work paves the way for the detection of fractional statistics in cold atoms through edge signatures.

*Introduction* — The interplay of topology and interactions leads to fascinating phases of matter, such as the fractional quantum Hall (FQH) states, which host fractionalized anyonic excitations. The progress in engineering artificial gauge fields [1, 2] and topological bands [3] has raised the hope of realizing FQH states of ultracold atoms. Specifically, realistic protocols for the preparation of FQH states were proposed [4–12], based on the quasi-adiabatic evolution of a small ensemble of neutral atoms loaded into an optical lattice. In this context, extracting the universal signatures of FQH states is an important goal and great challenge; theoretical proposals in this direction have mostly focused on the measurement of the Hall response [13–16], central charge [17], and the anyonic properties of quasiholes [18–23]. Recently, a two-particle bosonic Laughlin state was identified in an optical lattice [24], where local density measurements permitted the observation of key bulk signatures, including a nearly quantized Hall conductivity and vortex-like correlations.

Edge states are a fundamental hallmark of topological matter. In FQH systems, they form one-dimensional conduction channels, which are well captured by the chiral Luttinger liquid theory in the low-energy limit [25]. FQH edge modes are responsible for a wealth of quantum coherent phenomena in mesoscopic systems [26], and were instrumental in the observation of anyonic statistics [27, 28]. Despite the success of chiral Luttinger liquid theory in capturing these phenomena, microscopic details such as boundary effects can deeply affect the low-energy picture [29–33]. In numerical studies of few particles on a lattice, the expected gapless chiral edge spectrum was only reported in the presence of a smooth confining potential [34, 35]. Indeed, the FQH ground state is gapped in a confining box potential [14]. Thanks to the local probes accessible in optical-lattice experiments, the realization of the FQH effect in quantum gases may pro-

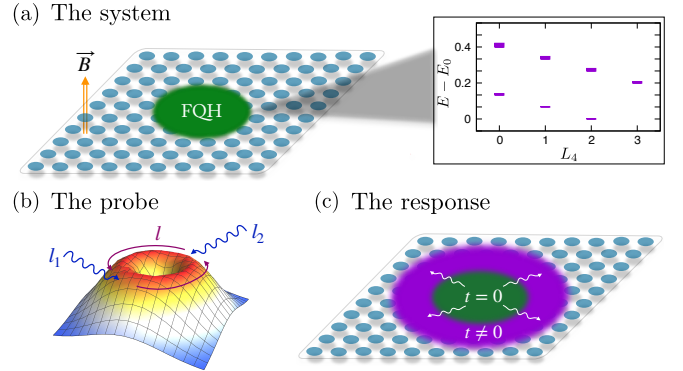


FIG. 1. (a) Fractional quantum Hall (FQH) droplet at the center of the Hofstadter-Bose-Hubbard lattice, with a sketch of the expected edge spectrum. (b) Spatial shape of the Laguerre-Gaussian (LG) laser field acting on the atoms, realized by interfering two beams with angular momentum  $l_1$  and  $l_2$ , and resulting in a transfer of angular momentum  $l = l_1 - l_2$ . (c) Response of the FQH droplet to the LG beams at resonance: edge states are populated, resulting in a detectable increase of the density at the edge of the droplet.

vide an opportunity to reveal the rich phenomenology of FQH edge modes. Promisingly, resolving individual edge states would provide a marker of topological order, permitting the unambiguous detection of non-Abelian FQH states [36–38]. While edge properties have been detected in weakly interacting cold atom settings [39–43], how to extract and resolve the edge spectrum of FQH states remains an open question.

In this work, we develop a spectroscopy protocol to extract the momentum-resolved edge spectrum of FQH states in ultracold quantum gases. Our proposal builds on Ref. [44] and is summarized in Fig. 1: two interfering Laguerre-Gaussian (LG) lasers transfer an angular mo-

mentum  $l$  and energy  $\hbar\omega$  to the system prepared in the FQH ground state of a lattice Hamiltonian. The absorption resonance is subsequently measured in-situ through local density measurements, by monitoring the displacement of the atomic density from bulk to edge. We numerically benchmark our protocol using the experimentally realized [24, 45] Hofstadter-Bose-Hubbard model, which supports a Laughlin  $1/2$  ground state [46–48]. By calculating the coupling matrix elements of our probe, we obtain the angular momentum resolved absorption spectrum and show that the expected chiral gapless edge mode is present in systems with as few as two particles. Interestingly, the LG matrix elements have an approximate selection rule beyond the exact symmetries of the Hamiltonian, which we attribute to the emergent continuous rotation symmetry of the ground state and low-energy excitations. This property allows us to extract the edge mode even when bulk and edge states are energetically mixed. We take advantage of this finding to study the behavior of the edge mode upon approaching the experimental configuration of Ref. [24]; there, the walls of the confining box nearly coincide with the edge of the FQH droplet, leading to a gapped edge mode, which lies higher in energy than the first bulk excitation [14]. The explicit time-dependent simulation of our protocol shows that the time necessary to detect a measurable transfer of density from bulk to edge is compatible with current experimental constraints. Our protocol could apply to other models of FQH states of ultracold atoms, including rotating atomic traps [43].

*Model* — We consider the Hofstadter-Bose-Hubbard (HBH) model, describing bosons hopping on the Harper-Hofstadter lattice [49] and interacting through an on-site Hubbard interaction,

$$\begin{aligned} \hat{H} = & -J \sum_{m,n} \left( \hat{b}_{m+1,n}^\dagger \hat{b}_{m,n} e^{i2\pi\alpha n} + \hat{b}_{m,n+1}^\dagger \hat{b}_{m,n} + \text{h.c.} \right) \\ & + \frac{U}{2} \sum_{m,n} \hat{b}_{m,n}^\dagger \hat{b}_{m,n} \left( \hat{b}_{m,n}^\dagger \hat{b}_{m,n} - 1 \right) \\ & + \sum_{m,n} V(m,n) \hat{b}_{m,n}^\dagger \hat{b}_{m,n}, \end{aligned} \quad (1)$$

where the operator  $\hat{b}_{m,n}$  ( $\hat{b}_{m,n}^\dagger$ ) destroys (creates) a boson at site  $(m,n)$ ,  $J$  is the tunneling energy,  $\alpha$  is the magnetic flux density,  $U > 0$  is the interaction strength, and  $V(m,n) = V_0 \left( (m - m_0)^2 + (n - n_0)^2 \right)$  is a confining potential ( $m_0, n_0$  are the coordinates of the lattice center). Throughout the paper, we work in the strong interaction regime  $U \gg J = 1$ , and use hardcore bosons in the numerics unless otherwise stated. For large  $U$  and  $\alpha < 1/3$ , this model hosts a fractional Chern insulator ground state [46–48], which is a lattice analog of the  $\nu = 1/2$  bosonic Laughlin state. A cold-atom implementation of this model was realized using two bosons in a box potential [24, 45], revealing signatures of the Laughlin FQH state [24].

We start by reviewing the known properties of the FQH

edge spectrum. In the low-energy limit, the edge modes of FQH states are described by a conformal field theory (CFT), whose nature depends on the topological order in the bulk [25, 36, 37]; for the Laughlin state considered in this paper, it coincides with the chiral Luttinger liquid. This powerful bulk-edge correspondence can be harnessed to identify FQH states from their low-energy spectrum in a geometry with edges; indeed, the edge spectrum reveals the universal counting of the CFT (the number of low-energy edge states for each momentum value). Extracting the edge spectrum is a non-trivial task, even numerically, especially for the small lattices accessible to numerics and experiments. Previous numerical studies have shown that a gapless chiral edge mode, whose counting matches the CFT expectation [34, 35], could be extracted from the energy spectrum in the presence of a smooth confining potential. Interestingly, this property is already present in two-boson systems, with corrections to the CFT counting due to finite particle number [35][50]. This is illustrated in Fig. 2(a), through the low-energy spectrum of two bosons in the HBH model in a weak harmonic trap. We use the eigenvalues of the modified  $C_4$  rotation operator [51] as good quantum numbers to highlight the chirality of the edge spectrum. The situation is different in a box potential: when the walls of the box coincide with the edge of the FQH droplet, the FQH ground state is gapped [13, 34], hence complicating the study of edge excitations. When the walls of the box are located far away from the droplet’s edge, the low-energy spectrum is gapless. However, as shown in Fig. 2(c), there is no structure permitting the extraction of the edge spectrum in this case. We now show how chiral edge properties can nonetheless be extracted in these relevant configurations, using a proper spectroscopic probe.

*Optical spectroscopy* — We propose to probe the FQH edge spectrum by using two Laguerre-Gaussian (LG) lasers, designed to induce a transition from the prepared FQH ground state to low-energy edge excitations. This transition involves a transfer of angular momentum  $l$ , and energy  $\hbar\omega$ , which are conveniently controlled by the pair of LG beams [52] (see Fig. 1). This is in contrast with the detection scheme of Refs. [31, 53], where the dispersion relation is extracted through a Fourier transform of the particle density following a quench. Such a LG-driving scheme was initially proposed in Ref. [44] to probe the edge spectrum of integer QH states. Beyond the strongly-interacting nature of the FQH state treated in this work, the small system sizes envisaged to realize FQH states in experiments results in a highly discretized spectrum. Our proposed scheme takes these key properties into account, and we discuss their consequences on the resulting absorption spectrum.

Inspired by Ref. [44], we consider a spectroscopic probe that results from the interference of two LG beams. The LG modes are solutions of the cylindrical-symmetric

wave equation, and take the following form

$$LG(r, \theta) \propto \left(\frac{r}{r_0}\right)^{|l|} e^{-\frac{r^2}{2r_0^2}} e^{i\theta l} \equiv f_l(r)e^{i\theta l}, \quad (2)$$

where the integer  $l$  represents the quantum of orbital angular momentum carried by each photon. As shown in Fig. 1(b), such an optical mode has a spatial vortex structure, with a ring of maximum amplitude that can be adjusted to optimize the edge response. The interference of two such LG beams, with frequencies  $\omega_1, \omega_2$  and angular momenta  $l_1, l_2$ , produces a time-periodic potential acting on the atoms,

$$\hat{O}_l(t) = 2\epsilon \sum_j f_l(r_j) \cos(\omega t + \theta_j l) \hat{b}_j^\dagger \hat{b}_j, \quad (3)$$

where  $j$  sums over the lattice sites,  $\theta_j$  is the polar angle at  $j$ ,  $\omega = \omega_2 - \omega_1$  and  $l = l_2 - l_1$ . The strength of the probe  $\epsilon$  can be taken small enough to treat the driving field within linear response.

To predict allowed transitions, we calculate the coupling of the FQH ground state  $\psi_0$  to excitations  $\psi_n$  through the LG drive, i.e. the coupling matrix elements

$$I_n = \sum_j \langle \psi_n | f_l(r_j) e^{i\theta_j l} \hat{b}_j^\dagger \hat{b}_j | \psi_0 \rangle. \quad (4)$$

We calculate the low-energy eigenstates of  $\hat{H}$  for a system of  $N = 2$  hard-core bosons on a  $10 \times 10$  lattice with magnetic flux  $\alpha = 1/8$  using exact diagonalization (ED). The corresponding low-energy spectrum and matrix elements  $I_n$  are represented in Fig. 2 for a harmonic and a box potential, respectively. In both cases, the matrix elements exhibit a chiral branch at  $l < 0$ , and two isolated gapped states at  $l = 1$  and  $l = 2$ . We interpret the gapless  $l < 0$  branch as the chiral edge mode, in agreement with the expectation that the sign of orbital angular momentum injected by the probe should match the chirality of the edge boson. Conversely, the  $l > 0$  signal is interpreted as low-energy bulk excitations, which could correspond to the magneto-roton mode [54]. While the maximum value of  $|l|$  in the edge mode is dictated by the lattice size (here, the  $10 \times 10$  box), giving rise to a large number of low-energy edge states, the number of bulk magneto-roton excitations is equal to the number of particles [55, 56] (see Appendix E). The analysis of density profiles (below in the main text and in Appendix D) corroborates this interpretation of negative and positive  $l$  states as edge and bulk states, respectively.

Interestingly, the LG probe identifies a chiral branch even when no structure can be extracted from the low-energy ED spectrum. This is illustrated in Figs. 2(c) and (d), for a small droplet located within a large  $10 \times 10$  box. This behavior originates from an approximate selection rule, associated with the approximate conservation of the angular momentum  $l$ . While the discrete  $C_4$  rotation symmetry of our lattice model guarantees the conservation of  $l$  modulo 4, in the continuum limit  $\alpha \ll 1$ ,

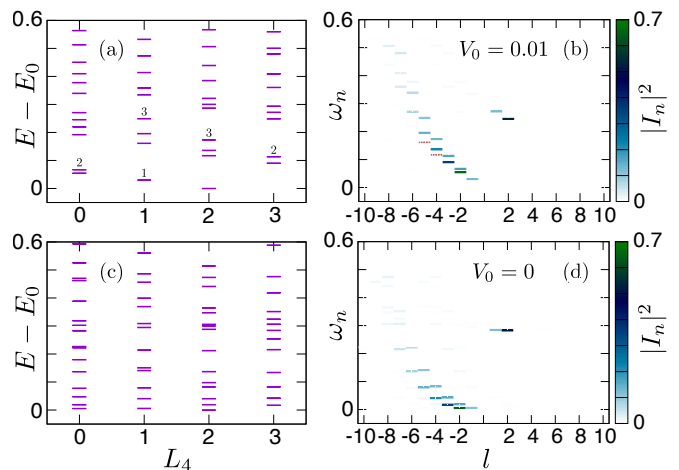


FIG. 2. Low-energy spectrum (a, c) and corresponding coupling matrix elements (b, d) for a system of 2 hardcore bosons in the HBH model at flux density  $\alpha = 1/8$ , in a  $10 \times 10$  box, with (a, b) or without (c, d) a harmonic potential of strength  $V_0 = 0.01$ . While the presence of the harmonic potential is necessary to distinguish the edge branch in the energy spectrum, the matrix elements  $I_n$  reveal the edge branch either way. The numbers in (a) indicate the number of states in each small “cluster”, which matches the CFT counting with finite particle number correction. In some clusters, one of the states [red dashed line in (b)] has a coupling amplitude 10 times smaller than the others.

the continuous rotation symmetry is recovered, leading to the conservation of  $l$ . For a flux  $\alpha = 1/8$ , coupling matrix elements that satisfy the conservation of  $l \bmod 4$  but not the conservation of  $l$  are two orders of magnitude smaller than those that do. Even for the experimentally relevant value  $\alpha = 1/4$ , this ratio is larger than 40. See Appendix A for more details on the influence of  $\alpha$  on the approximate conservation of angular momentum. Overall, the absorption spectra in Figs. 2(b) and (d) show that the addition of a weak harmonic potential increases the velocity of the chiral edge mode, such that its winding becomes visible in the folded energy spectrum [Fig. 2(a)].

We have chosen the value  $r_0 = 2$  for the Gaussian extension of the probe such that  $f_l(r)$  remains non-zero both in the bulk and a few magnetic lengths outside the edge of the FQH droplet, at least for  $|l| \leq 5$ . This is a necessary condition for the corresponding matrix elements to be non-zero, due to the different density profiles of the ground state and low-energy excited states, whose spatial extension increases with increasing energy (see Appendix D). Naturally, the optimal value of  $r_0$  depends on the size of the droplet; in larger droplets, it is especially useful to optimize  $r_0$  for different values of  $l$ , taking into account the respective edge and bulk nature of  $l < 0$  and  $l > 0$  states (see Appendix E).

*Connection to the Harvard experiment* — We now apply our spectroscopy protocol to the experimental setup of Léonard et al. [24]. In this realization, where  $N = 2$  interacting ( $U = 8.1J$ ) bosons are confined to a  $4 \times 4$  box

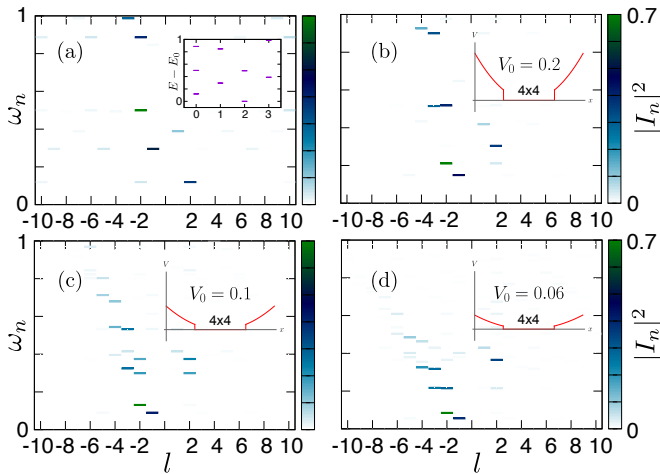


FIG. 3. Absorption spectra for  $N = 2$  interacting bosons ( $U = 8.1J$ ) on a  $10 \times 10$  HBH lattice with flux  $\alpha = 0.25$ , and different trap configurations, keeping  $V_0 = 0$  in the central  $4 \times 4$  portion of the lattice. (a) Harvard experiment configuration [24], with infinite walls around the  $4 \times 4$  box. The inset shows the corresponding energy spectrum. (b-d) Harmonic potential of respective strength  $V_0 = 0.2, 0.1, 0.06$ . Upon lowering the potential in the outer box, the bulk gap ( $l = 2$  signal) increases, while the edge branch ( $l < 0$ ) becomes gapless. Note the presence of a weak spurious signal at  $l = 2$ , at the same energy as the  $l = -2$  edge signal, due to the imperfect conservation of  $l$  in our lattice system.

with hard walls on the HBH lattice, a FQH ground state was identified within a flux window  $0.24 < \alpha < 0.3$ . Focusing on  $\alpha = 0.25$ , we show our probe's matrix elements for this experimental configuration in Fig. 3(a). The absorption spectrum is gapped, and the lowest energy excitation appears at  $l = 2$ . These features are compatible with the spectrum of a FQH state, whose edge mode is gapped due to the small size of the box. To confirm this interpretation, we release the FQH state into a  $10 \times 10$  box, by lowering the potential strength in the outer box from infinite to a harmonic potential of strength  $V_0$ . The corresponding absorption spectrum is displayed in Fig. 3, with the trap shape drawn as an inset. Upon releasing the walls of the  $4 \times 4$  box, the  $l < 0$  edge branch goes down and becomes gapless, while the  $l = 2$  bulk gap state increases in energy. We have systematically studied the effect of a change in box size on the absorption spectrum in Appendix C: generically, in a large box, the FQH droplet recovers a gapless edge mode, and its bulk gap increases until it reaches its thermodynamic value. Conversely, when the size of the box is reduced, the bulk gap decreases and eventually closes, marking a phase transition. Overall, our calculations show that increasing the size of the quantum-simulation box could permit the observation of a chiral gapless edge mode in ongoing experiments, even in two-atom droplets.

*Extracting the edge spectrum from in-situ density measurements* — We now show how to obtain the absorption spectrum studied in the previous paragraphs using

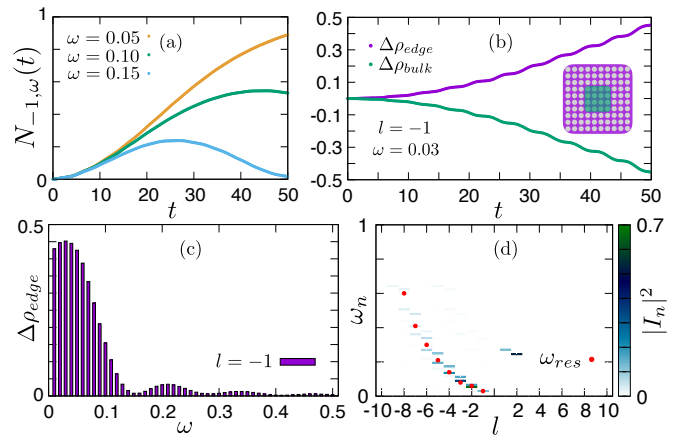


FIG. 4. Time evolution of 2 hardcore bosons on a  $10 \times 10$  HBH lattice with flux  $\alpha = 1/8$  and a harmonic trap of strength  $V_0 = 0.01$ , upon a LG drive of amplitude  $\epsilon = 0.05$ . (a) Excitation fraction as defined in Eq. (5), for an injected angular momentum  $l = -1$ . (b) Density variation at the edge and at the bulk, for  $l = -1$  angular momentum injected, at resonance  $\omega = 0.03$ . (c) Increment of the density at the edge evaluated at  $t^* = 50\hbar/J$  (d) Chiral branch retrieved by the protocol in the  $l < 0$  region, up to  $l = -8$ . Dots ( $\omega_{res}$ ) are the resonance frequencies obtained by density measurements, whereas the background color plot indicates the coupling matrix elements.

observables accessible to cold atom experiments.

Let us first address the time-dependent behavior of the excitation fraction:

$$N_{l,\omega}(t) = 1 - |\langle \psi(t) | \psi_0 \rangle|^2. \quad (5)$$

Due to its well-defined angular momentum  $l$ , our LG probe only couples the ground state to a handful of excited states at most, as observed in our numerical analysis of transition matrix elements  $I_n$ . As a result, the LG drive induces an effective two-level coupling for each value of  $l$ . Using unitary time-evolution of the FQH ground state subjected to the LG drive, we numerically observe Rabi oscillations, whose amplitude is maximal at the resonance frequency  $\omega = \omega_{res}$ ; see Fig. 4(a).

We propose to detect the resonant excitations through local density measurements, which are experimentally accessible using a quantum gas microscope [24, 45]. Indeed, following the excitation of chiral edge states, we expect that the density profile will change in order to populate the external rings outside the bulk. We define the instantaneous density at the edge as

$$\Delta \rho_{edge}(t) = \sum_{j \in edge} \rho_j(t) - \rho_j(0), \quad (6)$$

where  $\rho_j$  is the local density on site  $j$ , and we have defined the complementary bulk and edge regions [green and purple regions in the inset of Fig. 4(b)] from the density profile in the ground state (see Appendix D). The time-dependent behavior of  $\Delta \rho_{edge}(t)$ , as obtained using

numerical time-evolution is shown in Fig. 4(b), confirms the migration of the particle density from bulk to edge for a negative injected angular momentum. Figure 4(c) shows the values of  $\Delta\rho_{edge}$  at different probing frequencies  $\omega$ , taken after an observation time  $t^* = 50\hbar/J$ : we can clearly distinguish the resonance around  $\omega = 0.03$  for  $l = -1$ . Iterating this procedure for different values of the injected angular momentum  $l$ , we retrieve the chiral edge spectrum in Fig. 4(d). We point out that a realistic observation time  $t^* \sim 10 - 100\hbar/J$  leads to a clear signal  $\Delta\rho_{edge}(t^*) \sim 0.1 - 1$ , which can be detected in-situ using a quantum gas microscope [24]. While our scheme is particularly well suited to detect edge resonances, we note that it could be designed to probe the bulk (magneto-roton) excitations at  $l > 0$ . We also verified the ability of our protocol to detect edge signals in the experimental configuration of Ref. [24]; see Appendix B.

*Discussion* — Our work indicates that the chiral edge branch of atomic FQH droplets can be probed by measuring the local density following a Laguerre-Gaussian drive. Our method is especially well suited to probe the few-atom droplets addressed by ongoing experiments, and reveals the angular momentum resolved spectrum in lattices with as few as 2 particles. We have verified the validity of our results beyond this limit, for 3 or 4 particles, where we can still address very dilute systems (see Appendix E). Overall, our results show that increasing the lattice size beyond the small boxes realized so far in experiments [24] would permit the extraction of a gapless edge mode even in two-particle systems.

Beyond experimental purposes, the calculation of LG

matrix elements is a convenient theoretical tool to extract the angular momentum of energy states, especially in lattice systems without continuous rotation symmetry. It has allowed us to distinguish bulk and edge states even when they are energetically mixed, to track the evolution of the bulk gap and of the velocity of the edge branch upon changing the confining conditions.

Finally, our method is promising in view of identifying the fractional statistics of anyonic excitations from edge signatures (see also Ref. 18). Indeed, we have found that the number of states detected by our LG probe for each value of the angular momentum  $l$  matches the CFT counting for a free chiral boson (with corrections due to the small particle number [35]), which is expected to describe the edge of a Laughlin droplet. We note, however, that longer probing times will be needed to resolve the resonances occurring at the same  $l$ , since they are very close in energy. Moreover, some of the non-zero matrix elements have a very small amplitude (10 to 100 times smaller than the maximal signal), which could impede their detection. We leave to future work the optimization of the microscopic model and probe shape in view of resolving the universal CFT counting of FQH droplets.

*Acknowledgments* — We thank Jean Dalibard, André Eckardt, Fabian Grusdt, Adolfo G. Grushin, Markus Holzmann, Julian Léonard, Felix Palm and Botao Wang for insightful discussions. C.R. acknowledges support from ANR through grant ANR-22-CE30-0022-01. Work in Brussels is supported by the FRS-FNRS (Belgium), the ERC Starting Grants TopoCold and LATIS, and the EOS project CHEQS.

- 
- [1] J. Dalibard, F. Gerbier, G. Juzeliūnas, and P. Öhberg, *Rev. Mod. Phys.* **83**, 1523 (2011).
  - [2] N. Goldman, G. Juzeliūnas, P. Öhberg, and I. B. Spielman, *Reports on Progress in Physics* **77**, 126401 (2014).
  - [3] N. R. Cooper, J. Dalibard, and I. B. Spielman, *Rev. Mod. Phys.* **91**, 015005 (2019).
  - [4] M. Popp, B. Paredes, and J. I. Cirac, *Phys. Rev. A* **70**, 053612 (2004).
  - [5] N. R. Cooper and J. Dalibard, *Phys. Rev. Lett.* **110**, 185301 (2013).
  - [6] N. Y. Yao, A. V. Gorshkov, C. R. Laumann, A. M. Läuchli, J. Ye, and M. D. Lukin, *Phys. Rev. Lett.* **110**, 185302 (2013).
  - [7] F. Grusdt, F. Letscher, M. Hafezi, and M. Fleischhauer, *Phys. Rev. Lett.* **113**, 155301 (2014).
  - [8] Y.-C. He, F. Grusdt, A. Kaufman, M. Greiner, and A. Vishwanath, *Phys. Rev. B* **96**, 201103 (2017).
  - [9] C. Repellin, T. Yefsah, and A. Sterdyniak, *Phys. Rev. B* **96**, 161111 (2017).
  - [10] J. Motruk and F. Pollmann, *Phys. Rev. B* **96**, 165107 (2017).
  - [11] A. Hudomal, N. Regnault, and I. Vasić, *Phys. Rev. A* **100**, 053624 (2019).
  - [12] B. Michen, C. Repellin, and J. C. Budich, *Phys. Rev. Res.* **5**, 023100 (2023).
  - [13] C. Repellin and N. Goldman, *Phys. Rev. Lett.* **122**, 166801 (2019).
  - [14] C. Repellin, J. Léonard, and N. Goldman, *Phys. Rev. A* **102**, 063316 (2020).
  - [15] J. Motruk and I. Na, *Phys. Rev. Lett.* **125**, 236401 (2020).
  - [16] Z.-P. Cian, H. Dehghani, A. Elben, B. Vermersch, G. Zhu, M. Barkeshli, P. Zoller, and M. Hafezi, *Phys. Rev. Lett.* **126**, 050501 (2021).
  - [17] F. A. Palm, S. Mardazad, A. Bohrdt, U. Schollwöck, and F. Grusdt, *Phys. Rev. B* **106**, L081108 (2022).
  - [18] N. R. Cooper and S. H. Simon, *Phys. Rev. Lett.* **114**, 106802 (2015).
  - [19] M. Račiūnas, F. N. Ünal, E. Anisimovas, and A. Eckardt, *Phys. Rev. A* **98**, 063621 (2018).
  - [20] R. O. Umucal ilar, E. Macaluso, T. Comparin, and I. Carusotto, *Phys. Rev. Lett.* **120**, 230403 (2018).
  - [21] E. Macaluso, T. Comparin, R. O. Umucal ilar, M. Gerster, S. Montangero, M. Rizzi, and I. Carusotto, *Phys. Rev. Res.* **2**, 013145 (2020).
  - [22] B. Wang, X.-Y. Dong, and A. Eckardt, *SciPost Phys.* **12**, 095 (2022).
  - [23] X. Li, B. Jaworowski, M. Haque, and A. E. B. Nielsen, (2023), [arXiv:2305.18364](https://arxiv.org/abs/2305.18364) [cond-mat.mes-hall].
  - [24] J. Léonard, S. Kim, J. Kwan, P. Segura, F. Grusdt,

- C. Repellin, N. Goldman, and M. Greiner, (2022), [10.48550/2210.10919](https://arxiv.org/abs/10.48550/2210.10919).
- [25] X. G. Wen, *Phys. Rev. B* **41**, 12838 (1990).
- [26] C. Bäuerle, D. C. Glatzli, T. Meunier, F. Portier, P. Roche, P. Roulleau, S. Takada, and X. Waintal, *Reports on Progress in Physics* **81**, 056503 (2018).
- [27] J. Nakamura, S. Liang, G. C. Gardner, and M. J. Manfra, *Nature Physics* **16**, 931 (2020).
- [28] H. Bartolomei, M. Kumar, R. Bisognin, A. Marguerite, J.-M. Berroir, E. Bocquillon, B. Plaçais, A. Cavanna, Q. Dong, U. Gennser, Y. Jin, and G. Fève, *Science* **368**, 173 (2020).
- [29] E. Macaluso and I. Carusotto, *Phys. Rev. A* **96**, 043607 (2017).
- [30] R. Fern and S. H. Simon, *Phys. Rev. B* **95**, 201108 (2017).
- [31] X.-Y. Dong, A. G. Grushin, J. Motruk, and F. Pollmann, *Physical review letters* **121**, 086401 (2018).
- [32] A. Nardin and I. Carusotto, (2022), [10.48550/ARXIV.2203.02539](https://arxiv.org/abs/10.48550/ARXIV.2203.02539).
- [33] B. Oblak, B. Lapiere, P. Moosavi, J.-M. Stéphan, and B. Estienne, “Anisotropic quantum hall droplets,” (2023), [arXiv:2301.01726 \[cond-mat.mes-hall\]](https://arxiv.org/abs/2301.01726).
- [34] J. A. Kjäll and J. E. Moore, *Phys. Rev. B* **85**, 235137 (2012).
- [35] W.-W. Luo, W.-C. Chen, Y.-F. Wang, and C.-D. Gong, *Phys. Rev. B* **88**, 161109 (2013).
- [36] G. Moore and N. Read, *Nuclear Physics B* **360**, 362 (1991).
- [37] X.-G. Wen, *Phys. Rev. Lett.* **70**, 355 (1993).
- [38] M. Milovanović and N. Read, *Phys. Rev. B* **53**, 13559 (1996).
- [39] M. Mancini, G. Pagano, G. Cappellini, L. Livi, M. Rider, J. Catani, C. Sias, P. Zoller, M. Inguscio, M. Dalmonte, and L. Fallani, *Science* **349**, 1510 (2015).
- [40] B. K. Stuhl, H.-I. Lu, L. M. Ayccock, D. Genkina, and I. B. Spielman, *Science* **349**, 1514 (2015).
- [41] T. Chalopin, T. Satoor, A. Evrard, V. Makhlov, J. Dalibard, R. Lopes, and S. Nascimbene, *Nature Physics* **16**, 1017 (2020).
- [42] C. Braun, R. Saint-Jalm, A. Hesse, J. Arceri, I. Bloch, and M. Aidelsburger, “Real-space detection and manipulation of topological edge modes with ultracold atoms,” (2023), [arXiv:2304.01980 \[cond-mat.quant-gas\]](https://arxiv.org/abs/2304.01980).
- [43] R. Yao, S. Chi, B. Mukherjee, A. Shaffer, M. Zwierlein, and R. J. Fletcher, “Observation of chiral edge transport in a rapidly-rotating quantum gas,” (2023), [arXiv:2304.10468 \[cond-mat.quant-gas\]](https://arxiv.org/abs/2304.10468).
- [44] N. Goldman, J. Beugnon, and F. Gerbier, *Phys. Rev. Lett.* **108**, 255303 (2012).
- [45] M. E. Tai, A. Lukin, M. Rispoli, R. Schittko, T. Menke, Dan Borgnia, P. M. Preiss, F. Grusdt, A. M. Kaufman, and M. Greiner, *Nature* **546**, 519 (2017).
- [46] A. S. Sorensen, E. Demler, and M. D. Lukin, *Phys. Rev. Lett.* **94**, 086803 (2005).
- [47] M. Hafezi, A. S. Sørensen, E. Demler, and M. D. Lukin, *Phys. Rev. A* **76**, 023613 (2007).
- [48] M. Gerster, M. Rizzi, P. Silvi, M. Dalmonte, and S. Montangero, *Phys. Rev. B* **96**, 195123 (2017).
- [49] D. R. Hofstadter, *Phys. Rev. B* **14**, 2239 (1976).
- [50] For 2 particles, the counting for a free chiral boson CFT (1, 1, 2, 3, 5, 7 . . . ) is truncated down to (1, 1, 2, 2, 3, 3 . . . ).
- [51] T. Ozawa, H. M. Price, and I. Carusotto, *Phys. Rev. A* **92**, 023609 (2015).
- [52] H. He, M. E. J. Friese, N. R. Heckenberg, and H. Rubinsztein-Dunlop, *Phys. Rev. Lett.* **75**, 826 (1995).
- [53] B.-Y. Sun, N. Goldman, M. Aidelsburger, and M. Bukov, *PRX Quantum* **4**, 020329 (2023).
- [54] S. M. Girvin, A. H. MacDonald, and P. M. Platzman, *Phys. Rev. B* **33**, 2481 (1986).
- [55] C. Repellin, T. Neupert, Z. Papić, and N. Regnault, *Phys. Rev. B* **90**, 045114 (2014).
- [56] T. Jolicoeur, *Phys. Rev. B* **95**, 075201 (2017).

## SUPPLEMENTARY MATERIAL

### Appendix A: Influence of lattice effects on angular momentum selection rules

In the continuum, the conservation of continuous rotation symmetry results in a selection rule for the coupling matrix elements  $I_n$  defined in Eq. (4), which would allow the detection of a chiral edge branch with unbounded angular momentum in the absorption spectrum. In a square lattice with discrete rotation symmetry, in principle, we expect non-zero matrix elements  $I_n = \langle \psi_{L'} | \hat{O}_l | \psi_L \rangle$  whenever  $L' = L + l(\text{mod})4$ , where  $L$  and  $L' \in \mathbb{Z}_4$  are the rotation eigenvalues of two Hamiltonian eigenstates. Yet, as we have observed in the main text, many matrix elements satisfying this discrete rotation selection rule are negligible. This reveals the approximate continuous rotation symmetry, which becomes exact in the continuum limit  $\alpha \ll 1$  of the Hofstadter Hamiltonian. To further illustrate this phenomenon, we show the evolution of matrix elements upon increasing the flux from  $\alpha = 0.12$  to  $\alpha = 0.22$  in Fig. 5. We note that the ground state remains a FQH state across this magnetic flux range, as denoted by the visible chiral edge branch at  $l < 0$  and bulk gap at  $l = 2$ . Figure 5(e) shows the sum over excited states of the  $l = -1$  matrix elements; it highlights the increase in amplitude of the spurious signal associated with  $l = -1 + 4p$ , where  $p$  is a non-zero integer (the biggest contribution comes from  $l = -5$ , as is visible in Fig. 5(d)).

### Appendix B: Time-dependent density measurements in the Harvard-experiment configuration

In the main text we presented the absorption spectra related to the experimental setup of Ref. [24]. We now apply our time-dependent protocol to test its robustness in real scenarios. We show again the absorption spectrum in the experimental configuration in Fig. 6(a) but this time on an extended energy scale. We note the presence of spurious states, associated with the imperfect conservation of angular momentum  $l$  in this small lattice system. For example, the low-energy state previously identified as the bulk gap is present with its largest matrix element at  $l = 2$ , but it is also visible (with a much smaller amplitude) at  $l = -2$  and  $l = \pm 10$ . We might then worry that this spurious bulk signal at  $l = -2$  might obfuscate the extraction of the edge spectrum. Fortunately, our time-dependent density measurement protocol easily distinguishes edge and bulk signal, as is shown in Fig. 6(b), since the bulk-to-edge density transfer only occurs when the LG probe couples the ground state to an edge state.

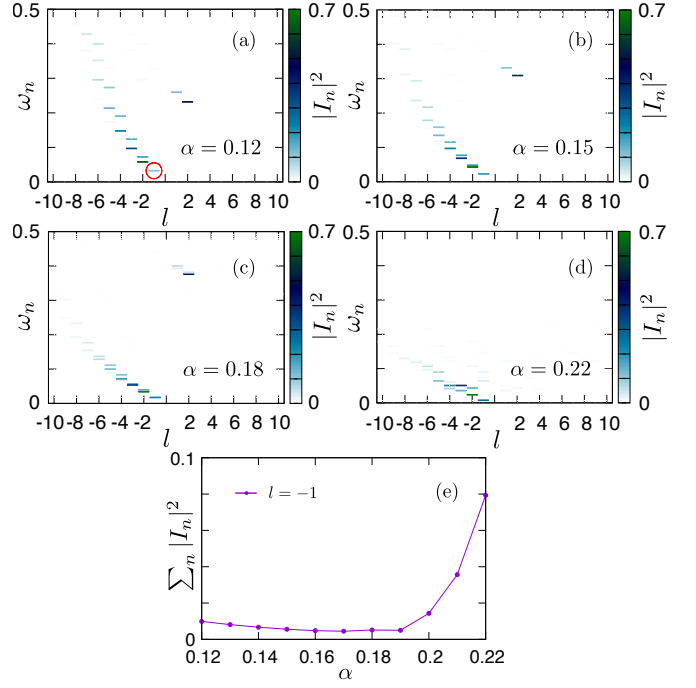


FIG. 5. (a-d) Coupling matrix elements of the LG probe for a system of  $N = 2$  bosons on a harmonically trapped ( $V_0 = 0.01$ )  $10 \times 10$  lattice with different flux densities  $\alpha$ . The LG beam has a radius  $r_0 = 2$ . (e) Sum of matrix elements in the sectors  $l = -1$  as a function of the flux density, excluding the red-circled, lowest energy state.

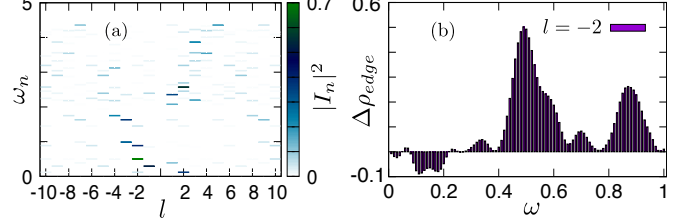


FIG. 6. (a) Absorption spectrum for  $N = 2$  bosons on a  $4 \times 4$  lattice with hard walls ( $V_0 = 0$ ), for a flux density  $\alpha = 0.25$  and on-site interaction  $U = 8.1J$ . The laser beam has a radius  $r_0 = 2$ . (b) Bulk to edge density transfer, as retrieved through the time-dependent protocol explained in the main text, probing the  $l = -2$  sector of the absorption spectrum in (a), showing the absence of bulk to edge transfer below  $\omega \simeq 0.4$

### Appendix C: Exploring the dilute to dense transition

In the main text we showed how a gapless edge mode can be detected in the absorption spectrum when we have a sufficiently dilute system (i.e. when the simulation box is larger than the FQH droplet). On the other hand we have seen how the chiral branch becomes gapped if the box size nearly coincides with the size of the FQH droplet, as in the experimental configuration [24] involving  $N = 2$  bosons in a  $4 \times 4$  box.

In Fig. 7, we show additional data illustrating this phe-



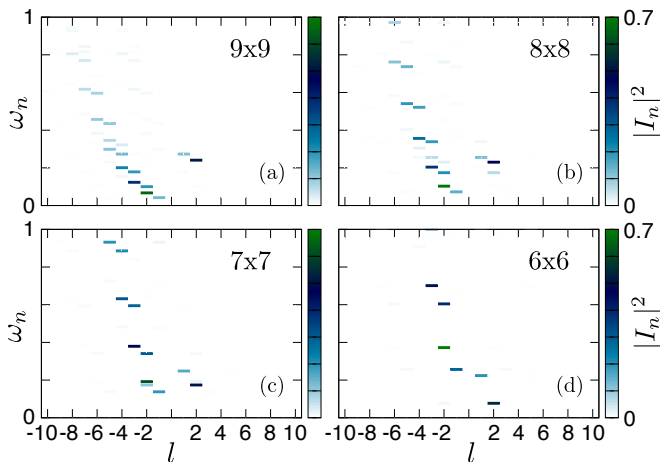


FIG. 7. (a)-(d) Absorption spectra for different lattice size, in the case of  $N = 2$  bosons and a flux density  $\alpha = 0.125$ , in a harmonic trap ( $V_0 = 0.01$ ) and a LG radius  $r_0 = 2$ . We observe a transition to a trivial phase for a 5x5 lattice (not shown).

nomenon, for hard wall boxes of different sizes, a droplet of  $N = 2$  bosons and a confinement potential of strength  $V_0 = 0.01$ , with a flux density  $\alpha = 0.125$ . We observe the chiral branch becoming steeper as the number of sites decreases, and the bulk gap (as tracked through the  $l = 2$  signal) decreasing accordingly. The closure of the bulk gap occurs between the 6x6 and the 5x5 boxes. We have verified that the ground state in the 5x5 box is a trivial state, which is adiabatically connected to the infinite trap limit (particles confined to the central site of the lattice).

Note that Fig. 5 illustrates the same phenomenon: there, the size of the FQH droplet changes, while the box size does not. As  $\alpha$  decreases, the radius of the FQH droplet increases (so that the density in the bulk satisfies Streda formula [14]), which results in a steeper edge mode and smaller bulk gap.

#### Appendix D: Local density patterns

Here, we show the local density of the ground state and edge excitations in our model. We consider  $N = 2$  bosons on a 10x10 square lattice with flux density  $\alpha = 0.125$ , confined in a harmonic trap of strength  $V_0 = 0.01$ . The ED spectrum in this configuration was shown in the main text, and is reproduced in Fig. 8(a). The eigenstates considered for the calculation of the density are marked with coloured dots. The ground state density profile in Fig. 8(b) shows a FQH droplet mostly confined to the center square, whereas the density of the excited states in Fig. 8(c)-(e) is more spread out. This behaviour explains the success of our detection protocol based on density measurement.

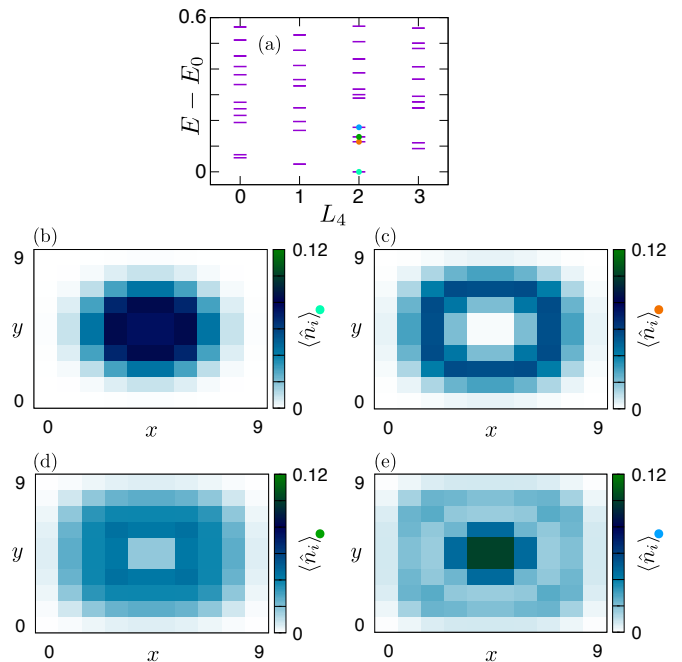


FIG. 8. (a) Energy spectrum for  $N = 2$  bosons in a 10x10 lattice, for a flux density  $\alpha = 0.125$  and a harmonic trap of strength  $V_0 = 0.01$ . The four coloured dots represent the state considered for the local density calculations in the next panels. (b) Local density profile of the ground state. (c)-(e) Local density profiles of three different excited states.

#### Appendix E: Absorption spectra for $N = 3, 4$ particles: chiral branch and magneto-roton mode

We now verify the validity of our protocol in systems with  $N = 3$  and  $N = 4$  particles, which are amenable to ED calculations in a lattice of respective size 10x10 and 8x8. A gapless edge branch requires the walls of the simulation box to lie sufficiently far outside of the FQH droplet, which prevents us from addressing systems with more than 4 particles with ED. For  $N = 3$ , we have used a flux density  $\alpha = 1/8$ , while for  $N = 4$ , we have used a larger value  $\alpha = 1/5$  to decrease the radius of the FQH droplet in this smaller box. In Fig. 9, we can identify the chiral edge branch in the  $l < 0$  region, in both cases. Let us now focus on the bulk excitations in the  $l > 0$  region. We find a low-energy mode with a cut-off at  $l_{max} = N$ , in agreement with our interpretation of this branch as the magneto-roton mode [55, 56].

The size of the FQH droplet scales with the number of particles  $N$ , so it is reasonable to expect an optimized chiral response by increasing the LG beam radius  $r_0$  compared to the  $N = 2$  case of the main text. In Fig. 9(a,c) the edge states are probed with the same  $r_0 = 2.5$ . Note that in order to emphasize the bulk response, it is useful to adjust the value of  $r_0$  to the value of injected angular momentum  $l$ ; specifically, we tuned  $r_0 = 2.0$  in order to have low-angular momentum injections acting mostly in the bulk region. This is especially important in sys-

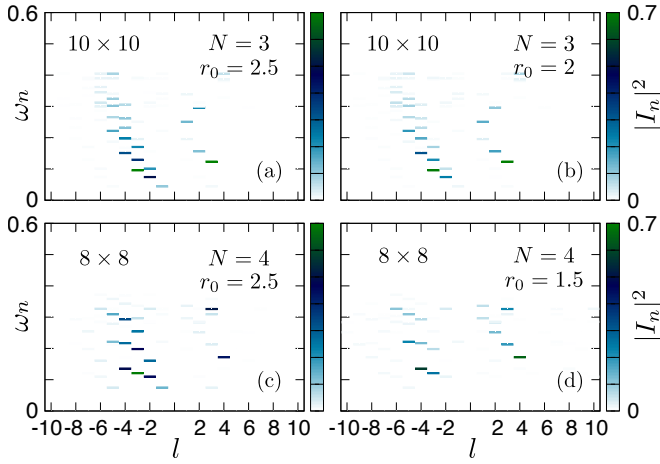


FIG. 9. Absorption spectra at different LG beam radii  $r_0$  for  $N = 3$  bosons in a  $10 \times 10$  lattice with a flux density  $\alpha = 1/8$  (a,b) and  $N = 4$  bosons in a  $8 \times 8$  lattice with a flux density  $\alpha = 1/5$  (c,d) trapped in a harmonic potential of strength  $V_0 = 0.01$ . We emphasize the chiral branch in the  $l < 0$  region when  $r_0 = 2.5$  for  $N = 3, 4$  particles (a,c), whereas we show the emergent magneto-roton mode in the  $l > 0$  region when the LG beam is acting deep in the bulk for low  $l$  values, namely when  $r_0 = 2$  for  $N = 3$  (b) and  $r_0 = 1.5$  for  $N = 4$  (d).

tems where the FQH droplet is larger (larger number of particles in particular).